

Self-Assembly versus Stepwise Synthesis: Heterometal–Organic Frameworks Based on Metalloligands with Tunable Luminescence Properties

Shu-Ran Zhang,^[a] Dong-Ying Du,^[a] Ke Tan,^[c] Jun-Sheng Qin,^[a] Hui-Qing Dong,^[b] Shun-Li Li,*^[b] Wen-Wen He,^[a] Ya-Qian Lan,*^[b] Ping Shen,^[a] and Zhong-Min Su*^[a]

Abstract: A new family of heterometal–organic frameworks has been prepared by two synthesis strategies, in which **IFMC-26** and **IFMC-27** are constructed by self-assembly and **IFMC-28** is obtained by stepwise synthesis based on the metalloligand (IFMC=Institute of Functional Material Chemistry). **IFMC-26** is a (3,6)-connected net and **IFMC-27** is a (4,8)-connected 3D framework. The metalloligands $\{\text{Ni}(\text{H}_4\text{L})\}(\text{NO}_3)_2$ are connected by binu-

clear lanthanide clusters giving rise to a 2D sheet structure in **IFMC-28**. Notably, **IFMC-26-Eu_xTb_y** and **IFMC-28-Eu_xTb_y** have been obtained by changing the molar ratios of raw materials. Owing to the porosity of **IFMC-26**,

Keywords: luminescence • metal–organic frameworks • metalloligands • self-assembly • stepwise synthesis

Tb³⁺@IFMC-26-Eu and **Eu³⁺@IFMC-26-Tb** are obtained by postencapsulating Tb^{III} and Eu^{III} ions into the pores, respectively. Tunable luminescence in metal–organic frameworks is achieved by the two kinds of doping methods. In particular, the quantum yields of heterometal–organic frameworks are apparently enhanced by postencapsulation of Ln^{III} ions.

Introduction

Metal–organic frameworks (MOFs) as a new class of crystalline materials have been the focus of significant interest due not only to their structural and chemical diversities but also to their functional properties and potential applications, for instance, gas storage, catalysis, separations, drug delivery, and so on.^[1,2] In recent years, MOFs have been especially promising as multifunctional luminescent materials,^[3] and much effort has been dedicated to this field.^[4] Both the inorganic and organic moieties in MOFs can provide the platform to generate luminescence, and metal–ligand charge-transfer-related luminescence within MOFs can add another

dimension to luminescent functionalities. Furthermore, the highly regular channel structures and controllable pore sizes of MOFs permit their application in some guest-molecule adsorption, which can also emit and/or induce luminescence.^[5] Besides, another technique can be used for the preparation of luminescent MOFs through combining quantum dots (QDs) with MOFs. Semiconductor QDs enhance light harvesting by MOFs through energy transfer from the QDs to the MOFs.^[6] Among these luminescent materials, lanthanide-based MOFs (LnMOFs) are receiving outstanding attention because of the advantages of the designability that allows fine-tuned luminescence properties.^[7] In general, Ln^{III} luminescent materials can be classified into two categories: 1) Ln^{III} ions coordinated directly to the organic linkers/sensitizers^[8] and 2) Ln^{III} ions encapsulated into porous MOFs.^[9] In this context, one can achieve the above-mentioned two types of LnMOFs, which possess adjustable luminescence properties by varying the molar ratios of raw materials of Ln^{III} ions, and postencapsulating Ln^{III} into porous MOFs. Nowadays, how to obtain tunable luminescent LnMOFs has become a prominent topic in fluorescent materials science.^[10]

It remains a labor-intensive endeavor to synthesize new families of MOF materials that possess a wide range of chemical functionalities and/or steric environments while retaining the crystallinity and porosity of the frameworks.^[11] Self-assembly, as a general approach, is accomplished only by careful selection of the metal, organic linker, and synthesis conditions.^[12] It has proven to be a powerful method for the design and construction of MOFs with diverse topologies and aesthetic beauty,^[13] but the mechanism is often masked by the common one-pot mixing procedure. Recent-

[a] Dr. S.-R. Zhang, Dr. D.-Y. Du, Dr. J.-S. Qin, Dr. W.-W. He, Dr. P. Shen, Prof. Z.-M. Su
Institute of Functional Material Chemistry
Faculty of Chemistry, Northeast Normal University
Changchun 130024, Jilin (P. R. China)
Fax: (+86) 431-85684009
E-mail: zmsu@nenu.edu.cn

[b] Dr. H.-Q. Dong, Prof. S.-L. Li, Prof. Y.-Q. Lan
Jiangsu Key Laboratory of Biofunctional Materials
College of Chemistry and Materials Science, Nanjing Normal University
Nanjing 210023, Jiangsu (P. R. China)
E-mail: lis132@nenu.edu.cn
yqlan@njnu.edu.cn

[c] Prof. K. Tan
Biological Scientific and Technical College
Changchun University
Changchun 130022, Jilin (P. R. China)

 Supporting information for this article is available on the WWW under <http://dx.doi.org/10.1002/chem.201301536>.

ly, Zhou, Zaworotko, Su, and co-workers^[14] have adopted a stepwise synthesis strategy to explore the synthetic mechanism. The synthesis strategy involves altering either 1) the metal node or 2) the organic linker after initial crystallization.^[13b] Stepwise synthesis of heterometal–organic frameworks is based on the synthesis of a metal complex that is subsequently connected to another metal ion.^[14d] Self-assembly and stepwise synthesis afford different means to modulate the physical and chemical properties of MOF structures, which may increase the use of MOFs as high-performance, tailor-made materials. Up to now, the exploration and investigation of the influences of self-assembly and stepwise synthesis on the structures and properties of these materials have rarely been investigated. It is still a significant challenge for targeted “design” and “control” tailor-made compounds with expected structures in synthesis chemistry and materials science.^[15]

Metalloligands, which are metal-containing complexes, have the coordination binding sites for their further coordination/binding with second metal ions and/or clusters.^[16] As highlighted recently, metalloligands are very appealing to target some functional MOFs as a result of their straightforward immobilization of functional sites, such as open metal sites, catalytically active metal sites, and photoactive metal sites, in the frameworks for adjusting their functional properties.^[17] Moreover, metalloligands with extra coordination sites (nitrogen and carboxyl groups) are ideal candidates for the construction of MOFs through stepwise synthesis.^[18] Hitherto, only a few studies have employed a stepwise synthesis strategy for the preparation of MOFs, especially based on metalloligands.

Our group has successfully constructed a novel coordination polymer with a special **scu** net under ionothermal synthesis, based on the ligand 4,4',4'',4'''-[2,2',2'',2''-[ethane-1,2-diylibis(azanetriyl)]tetrakis(methylene)tetrakis-(1H-benzo-[*d*]imidazole-2,1-diyl)}tetrakis(methylene)-tetrabenzoxic acid (H_4L).^[19a] Furthermore, we obtained a series of heterometallic Ln-based luminescent materials by the combination of hydrothermal and ionothermal methods for the first time.^[19b] As a continuation of our work, we took advantage of H_4L , Ni^{II} , and Ln^{III} ions through self-assembly, and metalloligands $\{Ni(H_4L)\}(NO_3)_2$ and Ln^{III} ions through stepwise synthesis in solvothermal reactions for heterometallic LnMOF preparation by taking the following factors into consideration. 1) Ln^{III} ions have a high affinity and prefer O to N donors, whereas the 3d metal ions have a tendency to coordinate with both N and O donors in self-assembly.^[20] Therefore, the coordination sites of H_4L can be correspondingly coordinated by Ln^{III} ions and transition metals. 2) Ni^{II} ions are chelated to nitrogen atoms from H_4L to form metalloligands. Meanwhile, uncoordinated polycarboxylate groups in metalloligands tend to coordinate with Ln^{III} , which benefits the construction of heterometallic LnMOFs by stepwise synthesis. 3) Ln^{III} ions display unique luminescence features, such as high luminescence quantum yield, narrow bandwidth, long-lived emission, and large Stokes shift. On the other hand, Ln^{III} ions have a predominantly electronic struc-

ture, for instance, the shielding of 4f orbitals from external perturbations.^[21]

We have obtained a series of heterometallic LnMOFs, $[Ni(L)Eu_xTb_y](NO_3)_5 \cdot 5H_2O \cdot 6DMA$ (DMA = dimethylacetamide; **IFMC-26-Eu_xTb_y**; $x=1$, $y=0$, **IFMC-26-Eu**; $x=0.5$, $y=0.5$, **IFMC-26-Eu_{0.5}Tb_{0.5}**; $x=0$, $y=1$, **IFMC-26-Tb** (IFMC = Institute of Functional Material Chemistry)) and $[Ni(L)La_2(NO_3)_3(dma)](NO_3)_2 \cdot 2H_2O \cdot 2DMA$ (**IFMC-27-La**) through self-assembly. Additionally, we have also achieved $[Ni(L)La(H_2O)(dmf)_2](NO_3)_3 \cdot 3H_2O \cdot DMF$ (**IFMC-28-La**) and $[Ni(L)Eu_xTb_y(H_2O)(dmf)_2](NO_3)_3 \cdot 3H_2O \cdot DMF$ (**IFMC-28-Eu_xTb_y**; $x=1$, $y=0$, **IFMC-28-Eu**; $x=0.6$, $y=0.4$, **IFMC-28-Eu_{0.6}Tb_{0.4}**; $x=0.5$, $y=0.5$, **IFMC-28-Eu_{0.5}Tb_{0.5}**; $x=0.4$, $y=0.6$, **IFMC-28-Eu_{0.4}Tb_{0.6}**; $x=0$, $y=1$, **IFMC-28-Tb**) by combining the metalloligand and Ln^{III} through stepwise synthesis. A series of characterizations was carried out on **IFMC-26–28**. By taking into account the excellent luminescence properties of Eu^{III} and Tb^{III} ions, the luminescence properties of **IFMC-26-Eu_xTb_y** and **IFMC-28-Eu_xTb_y** were investigated in the solid state at room temperature. Meanwhile, we postencapsulated Tb^{III} and Eu^{III} ions, respectively, into the pores of **IFMC-26-Eu** and **IFMC-26-Tb** and studied the influence of doping different Ln^{III} ions on fluorescence. To the best of our knowledge, this is the first time that the effects on the structures and properties of heterometallic LnMOFs attained through utilizing self-assembly and stepwise synthesis have been studied in the same system.

Results and Discussion

Herein, we have adopted two synthesis strategies for LnMOF preparation. The synthesis method for **IFMC-26** and **IFMC-27** is self-assembly, and for **IFMC-28** is stepwise. **IFMC-26-Eu** crystallizes in the orthorhombic space group *Pnna*. There is one Ni^{2+} ion, one Eu^{3+} ion, and one L^{4-} ligand in the crystallographically independent unit. The Ni atom is octahedrally coordinated by six nitrogen atoms from one bridging L^{4-} ligand to form a metalloligand unit (Figure 1a). Eight carboxylate groups from six different L^{4-} ligands connect two Eu^{3+} ions to form a mode of $[Eu_2(CO_2)_8]$ (see the Supporting Information, Figure S1a). The metalloligand unit links the $[Eu_2(CO_2)_8]$ cluster to form an infinite 3D framework. In the 3D net, pairs of adjacent carboxylate ligands link four adjacent L^{4-} ligands by sharing four binuclear $[Eu_2(CO_2)_8]$ clusters to form a pore with a size of $19.30 \times 23.79 \text{ \AA}$ along the [010] direction (Figure 1b and c). From the topological analysis, each metalloligand unit is considered as a 3-connected node (Supporting Information, Figure S2a) and each $[Eu_2(CO_2)_8]$ cluster acts as a 6-connected node (Supporting Information, Figure S2b). **IFMC-26-Eu** is a (3,6)-connected framework with the Schläfli symbol of $(4^2 \cdot 8)(4 \cdot 8^2)(4^4 \cdot 8^{11})$ (Figure 1d). The thermal behavior of **IFMC-26-Eu** was studied by thermogravimetric analysis (TGA; Supporting Information, Figure S9a). Single-crystal X-ray analysis reveals that **IFMC-26-Tb** is isostructural to **IFMC-26-Eu**. We then took advantage of a mixture of

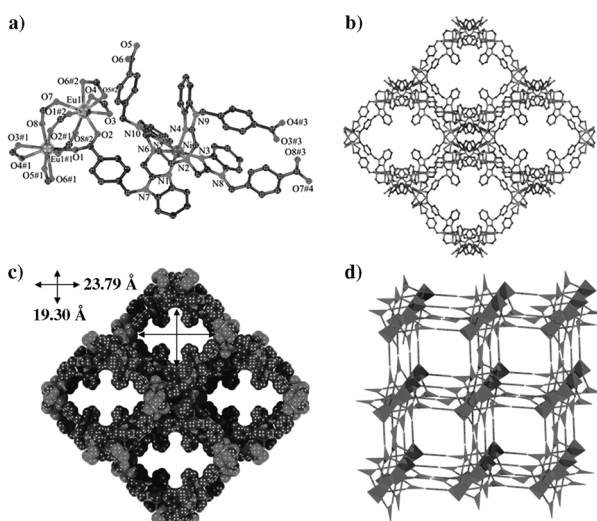


Figure 1. a) Coordination environments of the Ni^{II} and Eu^{III} centers in **IFMC-26-Eu**. Symmetry codes: #1: 0.5-x, 0.5+y, 0.5-z; #2: 0.5-x, 1-y, z; #3: 1-x, 1-y, 1-z; #4: 1-x, 0.5+y, 0.5+z. b,c) Ball-and-stick and space-filling representations of **IFMC-26-Eu** viewed from the [010] direction, respectively. All the hydrogen atoms are omitted for clarity. d) Polyhedral view of the (3,6)-connected topology network in **IFMC-26-Eu**.

Eu^{III} and Tb^{III} instead of Eu^{III} and obtained **IFMC-26-Eu_{0.5}Tb_{0.5}**. The experimental X-ray powder diffraction (XRPD) patterns of as-synthesized **IFMC-26-Eu_{0.5}Tb_{0.5}** and **IFMC-26-Tb** are in good agreement with the simulated diffraction pattern of **IFMC-26-Eu**, which indicates that the bulk materials have a (3,6)-connected 3D net framework similar to **IFMC-26-Eu** (Supporting Information, Figure S3). Therefore, only the structure of **IFMC-26-Eu** is described in detail.

As an extension of this work, we investigated the reaction of La(NO₃)₃ and H₄L under similar conditions and obtained **IFMC-27-La**. Interestingly, the structure of **IFMC-27-La** is different from that of **IFMC-26-Eu**. Single-crystal X-ray analysis reveals that **IFMC-27-La** crystallizes in the triclinic space group *P*̄*I*. The asymmetric unit of **IFMC-27-La** includes a Ni²⁺ ion, two kinds of La³⁺, an L⁴⁻ ion, three NO₃⁻ ions, and a coordinated DMA molecule. The coordination environments of the Ni atom and La atom are presented in Figure 2a. The Ni atom coordinates to six nitrogen atoms from the same L⁴⁻ ligand to form a twisted octahedral geometry [NiN₆]. There are two kinds of La atoms linked by carboxylate groups and NO₃⁻ to form a tetranuclear [La₄(CO₂)₈(NO₃)₆(dma)₂] cluster (Supporting Information, Figure S1b), in which La atoms exhibit two different coordination geometries. La₁ coordinates to five oxygen atoms from three L⁴⁻ ligands, four oxygen atoms from two NO₃⁻ ions, and one oxygen atom from coordinated DMA. La₂ is eight-coordinated by three oxygen atoms from three L⁴⁻ ligands and five oxygen atoms from four NO₃⁻ ions. Furthermore, the adjacent clusters are linked by the L⁴⁻ ligands to give a three-dimensional network. In addition, two adjacent L⁴⁻ ligands link each other through sharing two tetranuclear [La₄(CO₂)₈(dma)₂(NO₃)₆] to form a pore with the size of 3.72 ×

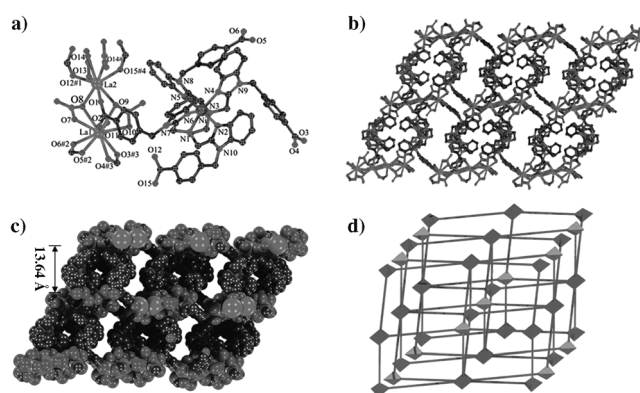


Figure 2. a) Coordination environments of the Ni^{II} and La^{III} centers in **IFMC-27-La**. Symmetry codes: #1: 1-x, 1-y, 1-z; #2: x, 1+y, z; #3: 1-x, -y, 2-z; #4: -1+x, y, z. b,c) Ball-and-stick and space-filling representations of **IFMC-27-La** viewed from the [100] direction, respectively. All the hydrogen atoms are omitted for clarity. d) Polyhedral view of the (4,8)-connected topology network in **IFMC-27-La**.

13.64 Å (Figure 2b and c). On further study into the structure of **IFMC-27-La**, we find that each tetranuclear metal cluster is surrounded by eight organic ligands. From the topological point of view, the [NiN₆] can be considered as a 4-connected node (Supporting Information, Figure S4a), whereas the tetranuclear lanthanum cluster is an 8-connected node (Supporting Information, Figure S4b). Therefore, the framework of **IFMC-27-La** is a rare (4,8)-connected fluorite (CaF₂) net with the Schläfli symbol of (4⁶)₂(4¹²•6¹²•8⁴) (Figure 2d). The XRPD patterns for **IFMC-27-La** are presented in Figure S5 (Supporting Information). The diffraction peaks of both simulated and as-synthesized patterns match well in key positions, thus indicating its phase purity. The thermal behavior of **IFMC-27-La** is presented in Figure S9b (Supporting Information).

It is advantageous to regard H₄L as the moiety of the metalloligand because H₄L belongs to the tetrapodand. We attained the metalloligand {Ni(H₄L)}(NO₃)₂ by the conventional synthesis reaction of H₄L and Ni^{II} in ethanol solution. Single-crystal X-ray analysis reveals that the metalloligand crystallizes in the monoclinic space group *C*2/c, and the asymmetric unit includes one Ni atom and one H₄L ligand. Each Ni atom is octahedrally coordinated by six nitrogen atoms from one ligand (Figure 3a), whereas the carboxylate groups from the H₄L are uncoordinated by any other atoms to form a discrete structure. The XRPD patterns for the metalloligand are shown in Figure S6 (Supporting Information). The diffraction peaks of both simulated and as-synthesized patterns match well in key positions, thus indicating phase purity. The thermal behavior of the metalloligand is displayed in Figure S9c (Supporting Information).

Taking into account the coordination environment of the metalloligand, we adopted stepwise synthesis by combining the metalloligand {Ni(H₄L)}(NO₃)₂ with La(NO₃)₃ and obtained **IFMC-28-La**. Notably, the structure of **IFMC-28-La** is completely different from those of **IFMC-26-Eu** and **IFMC-27-La**, displaying a 2D layer structure. Single-crystal X-ray

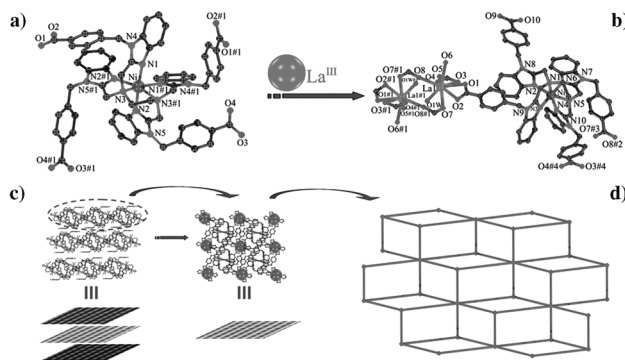
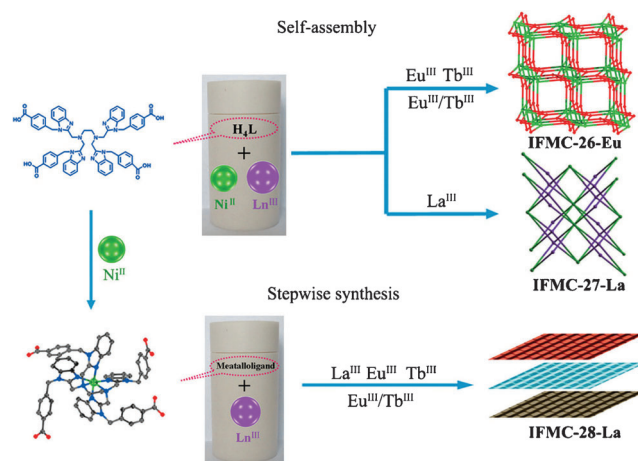


Figure 3. a) Coordination environment of the Ni^{II} center in the metalloligand. Symmetry code: #1: $-x, y, 0.5-z$. b) Coordination environments of the Ni^{II} and La^{III} centers in **IFMC-28-La**. Symmetry codes: #1: $1-x, -1-y, -z$; #2: $-1+x, 1+y, z$; #3: $-x, -y, -z$; #4: $x, 1+y, z$. c) Packing arrangement in **IFMC-28-La**. All the hydrogen atoms are omitted for clarity. d) Ball-and-stick view of the topological structure in **IFMC-28-La**.

diffraction studies reveal that **IFMC-28-La** crystallizes in the triclinic space group $P\bar{1}$. The crystallographically independent unit contains one metalloligand unit (Figure 3a), one La³⁺ ion, two coordinated dmf molecules, and two water molecules (Figure 3b). The La atom is nine-coordinated by six carboxylate oxygen atoms from four H₄L ligands, two oxygen atoms from coordinated dmf, and one water molecule, which generate a binuclear lanthanide cluster [La₂(CO₂)₆(dmf)₂(H₂O)₂] (Supporting Information, Figure S1c). Further study into the nature of this architecture reveals that **IFMC-28-La** displays a two-dimensional network in the *ab* plane, which is packed in the *bc* plane as described in Figure 3c. In addition, in each layer, each L⁴⁻ anion connects three binuclear lanthanide clusters, and each binuclear lanthanide cluster connects six L⁴⁻ ions. So the L⁴⁻ anion and binuclear lanthanide cluster are considered as 3- and 6-connected nodes (Supporting Information, Figure S7a and S7b). Such connectivity modes lead to a (3,6)-connected framework (Figure 3d).

The thermal behavior of **IFMC-28-La** was studied by TGA (Supporting Information, Figure S9d). Inspired by **IFMC-26-Eu_xTb_y**, we investigated the solvothermal reactions of Eu^{III}/Tb^{III} ions with different ratios by stepwise synthesis and obtained a family of LnMOFs: **IFMC-28-Eu**, **IFMC-28-Eu_{0.6}Tb_{0.4}**, **IFMC-28-Eu_{0.5}Tb_{0.5}**, **IFMC-28-Eu_{0.4}Tb_{0.6}**, and **IFMC-28-Tb**. On comparison of the experimental XRPD patterns of as-synthesized **IFMC-28-Eu**, **IFMC-28-Eu_{0.6}Tb_{0.4}**, **IFMC-28-Eu_{0.5}Tb_{0.5}**, **IFMC-28-Eu_{0.4}Tb_{0.6}**, and **IFMC-28-Tb** with the simulated diffraction pattern of **IFMC-28-La**, the very high degree of correspondence between the patterns indicates that the bulk materials have the same structure as **IFMC-28-La** (Supporting Information, Figure S8).

A series of LnMOFs, **IFMC-26**, **IFMC-27**, and **IFMC-28**, has been successfully achieved, which proves that we can design and control this system by using self-assembly and stepwise synthesis strategies (Scheme 1; Supporting Information, Scheme S1). To present the dimensions and shapes of the crystals, we have displayed their optical images taken



Scheme 1. Self-assembly and stepwise synthesis methods for the preparation of **IFMC-26-Eu**, **IFMC-27-La**, and **IFMC-28-La**.

by using a fluorescence microscope equipped with a CCD camera (Supporting Information, Figure S10). Self-assembly of the metal ions and clusters (generally termed as nodes) with organic linkers (connectors) of predetermined shapes can lead to the construction of MOFs with diverse structures. **IFMC-26-Eu** is a (3,6)-connected 3D porous framework, whereas **IFMC-27-La** is a (4,8)-connected 3D porous framework. Stepwise synthesis, facilitated by metalloligands, provides the capability to fine-tune the internal element coordination environments of MOFs and offers unprecedented opportunities to systematically evaluate and improve the performance of MOFs. **IFMC-28-Eu** and **IFMC-28-La** both display 2D layer structures that are distinctly different from that of **IFMC-26-Eu** and **IFMC-27-La**. The bright promise of the new metalloligand approach to assemble MOF materials with functional sites will initiate extensive research on the exploration and discovery of new functional MOFs. The two different synthesis methods discussed above exemplify a highly efficient and controllable approach to construct multifunctional MOFs.

The luminescence properties of **IFMC-26-Eu_xTb_y**, and **IFMC-28-Eu_xTb_y** in the solid state were investigated at room temperature. Excitation and emission spectra of H₄L are presented in Figure S11a (Supporting Information). **IFMC-26-Eu** yields an intense red luminescence when excited at 253 nm, which is assigned to the characteristic transitions $^5D_0 \rightarrow ^7F_J$ ($J=0-4$) of Eu^{III} ions (Figure 4a). Two intense emission bands at 616 and 700 nm correspond to $^5D_0 \rightarrow ^7F_2$ and $^5D_0 \rightarrow ^7F_4$, whereas the weaker emission bands at 592 and 653 nm originate from $^5D_0 \rightarrow ^7F_1$ and $^5D_0 \rightarrow ^7F_3$.^[22] Under excitation at 291 nm, **IFMC-26-Tb** exhibits typical fluorescence peaks at 489, 545, 584, and 621 nm, which are attributed to $^5D_4 \rightarrow ^7F_J$ ($J=3-6$) transitions^[23] (Figure 4b). The decay curve of transition $^5D_0 \rightarrow ^7F_2$ (616 nm) for **IFMC-26-Eu** is well-fitted by a biexponential function, which yields the lifetime value of $\tau_{ia}=11.04 \mu s$ (Supporting Information, Table S2). Similarly, for **IFMC-26-Tb**, the decay curve of transitions (545 nm) is well-fitted by a biexponential func-

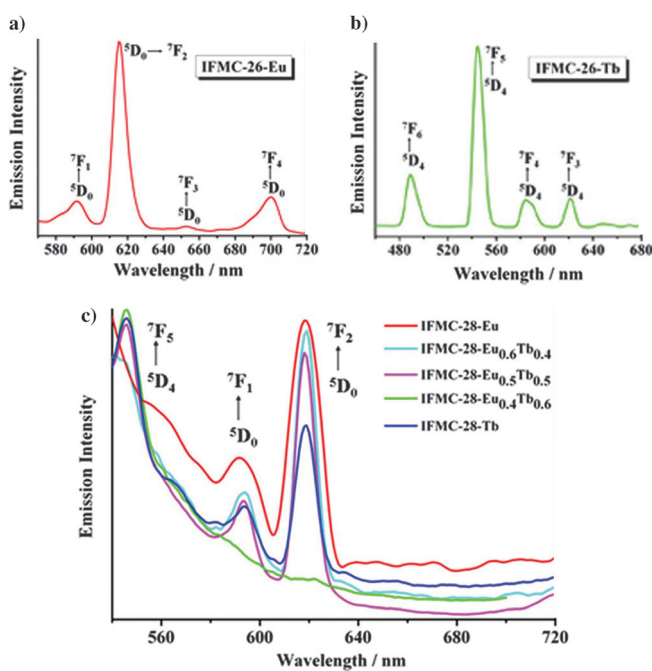


Figure 4. Emission spectra of a) IFMC-26-Eu, b) IFMC-26-Tb, and c) IFMC-28-Eu, IFMC-28-Eu_{0.6}Tb_{0.4}, IFMC-28-Eu_{0.5}Tb_{0.5}, IFMC-28-Eu_{0.4}Tb_{0.6}, and IFMC-28-Tb.

tion, to yield the lifetime value of $\tau_{ia}=6.53\ \mu\text{s}$ (Supporting Information, Table S2). It is expected that H₄L is a promising system for developing compounds with tunable luminescence properties. **IFMC-26-Eu_{0.5}Tb_{0.5}** was obtained successfully. As we expected, the intensities of red and green that originate from Eu^{III} and Tb^{III} emissions can be fine-tuned correspondingly (Supporting Information, Figure S12). Owing to the porosities of **IFMC-26-Eu** and **IFMC-26-Tb**, Ln^{III} ions were postencapsulated into the pores to obtain tunable luminescent materials by soaking the samples in DMA solutions of nitrate salts of Tb³⁺ and Eu³⁺ for 72 h. The successful Ln³⁺ loading was proved by the emission spectra of Tb³⁺@IFMC-26-Eu and Eu³⁺@IFMC-26-Tb (Supporting Information, Figure S13a and S13b). In addition, the crystalline integrities of **IFMC-26-Eu** and **IFMC-26-Tb** are retained as demonstrated by XRPD (Supporting Information, Figure S14). Notably, the lifetime of Eu^{III} in Tb³⁺@IFMC-26-Eu and Eu³⁺@IFMC-26-Tb shows longer Ln³⁺ lifetimes of 7.15 and 7.94 μs than that of **IFMC-26-Eu_{0.5}Tb_{0.5}** ($\tau_{ia}=6.33\ \mu\text{s}$). The lifetime of Tb^{III} in Tb³⁺@IFMC-26-Eu and Eu³⁺@IFMC-26-Tb shows longer Ln³⁺ lifetime of 6.72 and 8.57 μs than that of **IFMC-26-Eu_{0.5}Tb_{0.5}** ($\tau_{ia}=5.22\ \mu\text{s}$, Supporting Information, Table S2).

Excitation and emission spectra of the metalligand are shown in Figure S11b (Supporting Information). Upon excitation at 298 nm, **IFMC-28-Eu** displays narrow and characteristic peaks at 592, 619, 646, and 690 nm due to $^5\text{D}_0 \rightarrow ^7\text{F}_J$ ($J=0-4$) transitions of the Eu^{III} ion (Supporting Information, Figure S15a). The most intense emission at 619 nm is attributed to the $^5\text{D}_0 \rightarrow ^7\text{F}_2$ (electric-dipole) transition, which is hypersensitive to the coordination environment of the

Eu^{III} ion and implies a red emission light.^[24] The medium-strong emission band at 592 nm corresponds to the $^5\text{D}_0 \rightarrow ^7\text{F}_1$ (magnetic-dipole) transition, which is fairly insensitive to the environment of the Eu^{III} ion.^[21b] As shown in Figure S15a in the Supporting Information, the $^5\text{D}_0 \rightarrow ^7\text{F}_2$ transition is clearly stronger than the $^5\text{D}_0 \rightarrow ^7\text{F}_1$ transition with an intensity ratio of about 2.4 for $I(^5\text{D}_0 \rightarrow ^7\text{F}_2)/I(^5\text{D}_0 \rightarrow ^7\text{F}_1)$, thus indicating the absence of inversion symmetry at the Eu³⁺ site. **IFMC-28-Tb** yields a green luminescence under excitation at 298 nm, which is assigned to the characteristic transitions of $^5\text{D}_4 \rightarrow ^7\text{F}_J$ ($J=3-6$) of the Tb^{III} ions. The most intense emission band at 545 nm corresponds to $^5\text{D}_4 \rightarrow ^7\text{F}_5$, whereas the weaker emission band at 622 nm originates from $^5\text{D}_4 \rightarrow ^7\text{F}_3$ (Supporting Information, Figure S15b). Through tuning the ratios of Eu^{III}/Tb^{III}, the compounds **IFMC-28-Eu_xTb_y** ($x=0.6$, $y=0.4$, **IFMC-28-Eu_{0.6}Tb_{0.4}**; $x=0.5$, $y=0.5$, **IFMC-28-Eu_{0.5}Tb_{0.5}**; $x=0.4$, $y=0.6$, **IFMC-28-Eu_{0.4}Tb_{0.6}**) were successfully prepared. The intensities of red and green arising from Eu^{III} and Tb^{III} emissions can be shifted correspondingly. At the same time, the emission spectra were also recorded under similar conditions (Figure 4c). The emission band at 545 nm corresponds to the $^5\text{D}_4 \rightarrow ^7\text{F}_5$ transition of Tb^{III}, whereas the two emission bands at 592 and 619 nm originate from $^5\text{D}_0 \rightarrow ^7\text{F}_1$ and $^5\text{D}_0 \rightarrow ^7\text{F}_2$ transitions of Eu^{III}, respectively. The fluorescence lifetime of **IFMC-28-Eu** was measured from the decay curve of the $^5\text{D}_0 \rightarrow ^7\text{F}_2$ transition (619 nm) by fitting with a biexponential function, to yield the lifetime value of $\tau_{ia}=11.37\ \mu\text{s}$ (Supporting Information, Table S2). Meanwhile, the decay curve of $^5\text{D}_4 \rightarrow ^7\text{F}_5$ transitions (545 nm) for **IFMC-28-Tb** is well-fitted by a biexponential function, to yield a lifetime value of $\tau_{ia}=12.25\ \mu\text{s}$. Moreover, both the Eu^{III} and Tb^{III} decay curves in **IFMC-28-Eu_{0.6}Tb_{0.4}**, **IFMC-28-Eu_{0.5}Tb_{0.5}**, and **IFMC-28-Eu_{0.4}Tb_{0.6}** were also investigated. The Eu^{III} decay curves detected at $^5\text{D}_0 \rightarrow ^7\text{F}_2$ transitions (619 nm) of **IFMC-28-Eu_{0.6}Tb_{0.4}**, **IFMC-28-Eu_{0.5}Tb_{0.5}**, and **IFMC-28-Eu_{0.4}Tb_{0.6}** are well-fitted by biexponential functions with lifetime values of $\tau_{ia}=8.78$, 18.43, and 10.86 μs , respectively. Meanwhile, the Tb^{III} decay curves monitored at $^5\text{D}_4 \rightarrow ^7\text{F}_5$ transitions (545 nm) of **IFMC-28-Eu_{0.6}Tb_{0.4}**, **IFMC-28-Eu_{0.5}Tb_{0.5}**, and **IFMC-28-Eu_{0.4}Tb_{0.6}**, which are well-fitted by exponential functions, yield lifetime values of $\tau_{ia}=6.95$, 11.32, and 9.29 μs , respectively (Supporting Information, Table S2).

As shown above, the intensities of red and green originating from Eu^{III} and Tb^{III} ion emissions can be effectively tuned by changing the molar ratios of raw materials and postencapsulation. We have successfully achieved tunable luminescence in MOFs by two kinds of doping methods. Experimental inductively coupled plasma results are listed in Table S3 in the Supporting Information, which shows the corresponding contents of Eu^{III} and Tb^{III} in the final products. In addition, the quantum yields of **IFMC-26-Eu**, **IFMC-26-Tb**, **IFMC-26-Eu_xTb_y**, Tb³⁺@IFMC-26-Eu, Eu³⁺@IFMC-26-Tb, and **IFMC-28-Eu_xTb_y** are also presented in Table S3 (Supporting Information). Notably, the quantum yields of Tb³⁺@IFMC-26-Eu and Eu³⁺@IFMC-26-Tb are clearly higher than those of **IFMC-26-Eu_xTb_y** and **IFMC-28-**

Eu_xTb_y, which may be caused by the environments of Eu^{III} and Tb^{III}. In **Tb³⁺@IFMC-26-Eu** and **Eu³⁺@IFMC-26-Tb**, the postencapsulated Eu^{III} and Tb^{III} are free Eu³⁺ and Tb³⁺ ions, whereas Eu^{III} and Tb^{III} in **IFMC-26-Eu_xTb_y** and **IFMC-28-Eu_xTb_y** coordinate to the carboxylate groups of H₄L to form inorganic–organic hybrid materials. Moreover, the quantum yield of **IFMC-26-Eu_{0.5}Tb_{0.5}** is relatively higher than that in **IFMC-26-Eu**, **IFMC-26-Tb**, and **IFMC-28-Eu_xTb_y**, thereby revealing that the quantum yields are not only related to the molar ratios of Eu^{III} and Tb^{III} ions, but also to the structures of the complexes. As far as we know, this is the first time that the quantum yields for the ratio of Ln^{III} ions and postencapsulated Ln^{III} ions in LnMOFs have been compared.

Conclusion

A series of heterometallic LnMOFs has been prepared by self-assembly and stepwise synthesis. For the first time, a comparison has been made of the structures and properties of **IFMC-26–28**, which were obtained by the two different synthesis strategies. A wide variety of tunable luminescence was successfully attained not only by changing the molar ratios of Ln^{III} ions, but also through postencapsulating Tb^{III} and Eu^{III} ions into the pores of **IFMC-26-Eu** and **IFMC-26-Tb**, respectively. Notably, the quantum yields are clearly enhanced by postencapsulating Tb^{III} and Eu^{III} ions into the pores of **IFMC-26**. The quantum yields are related to both the molar ratios of Eu^{III} and Tb^{III} ions and the structures of the complexes. Therefore, such doping of heterometallic LnMOFs can be a strategy for preparing multifunctional luminescent materials. This work provides two different routes, self-assembly and stepwise synthesis, for the preparation of novel and functional heterometallic LnMOFs, as well as offering examples of crystalline materials with tunable luminescence. In addition, studies of the precisely tunable white-light emission of this system are currently under way.

Experimental Section

Synthesis of IFMC-26-Eu, [Ni(L)Eu](NO₃)·5H₂O·6DMA: H₄L (0.04 g, 0.36 mmol), NiCl₂·6H₂O (0.15 g, 0.63 mmol), Eu(NO₃)₃·6H₂O (0.05 g, 0.11 mmol), DMA (6 mL), and H₂O (4 mL) were sealed in a Teflon-lined stainless steel container. The container was heated to 120°C for 4 days, which resulted in light purple crystals that were isolated by washing with DMA and dried at room temperature. Yield: 54% based on H₄L. IR (KBr): $\tilde{\nu}$ =3419 (s), 3061 (m), 2935 (s), 1616 (s), 1543 (s), 1415 (s), 1262 (m), 1181 (m), 1107 (w), 1016 (m), 965 (w), 895 (w), 808 (m), 747 (s), 646 (w), 593 (m), 475 (w), 422 cm⁻¹ (m); elemental analysis calcd (%) for C₉₀H₁₁₆N₁₇O₂₂NiEu: C 54.08, H 5.86, N 11.92, Eu 7.60; found: C 54.02, H 5.92, N 11.98, Eu 7.53.

Synthesis of IFMC-26-Eu_{0.5}Tb_{0.5}: **IFMC-26-Eu_{0.5}Tb_{0.5}** was synthesized by a procedure similar to that used for **IFMC-26-Eu** with Eu(NO₃)₃·6H₂O (0.02 g, 0.05 mmol) and Tb(NO₃)₃·6H₂O (0.04 g, 0.09 mmol) instead of Eu(NO₃)₃·6H₂O (0.04 g, 0.09 mmol). The light purple crystals were isolated by washing with DMA and dried at room temperature. Yield: 58% based on H₄L. IR (KBr): $\tilde{\nu}$ =3385 (s), 2931 (s), 1628 (s), 1414 (s), 1298 (m), 1179 (m), 1084 (w), 1015 (m), 939 (w), 859 (m), 833 (w), 785 (m),

764 (s), 716 (m), 645 (w), 563 (w), 423 cm⁻¹ (m); elemental analysis calcd (%) for C₉₀H₁₁₆N₁₇O₂₂Ni Eu_{0.5}Tb_{0.5}: C 53.98, H 5.85, N 11.89, Eu 3.79, Tb 3.97; found: C 53.92, H 5.93, N 11.95, Eu 3.75, Tb 3.92.

Synthesis of IFMC-26-Tb, [Ni(L)Tb](NO₃)·5H₂O·6DMA: **IFMC-26-Tb** was synthesized by a procedure similar to that used for **IFMC-26-Eu** with Tb(NO₃)₃·6H₂O (0.05 g, 0.11 mmol) instead of Eu(NO₃)₃·6H₂O (0.05 g, 0.11 mmol). The light purple crystals were isolated by washing with DMA and dried at room temperature. Yield: 55% based on H₄L. IR (KBr): $\tilde{\nu}$ =3423 (s), 2937 (m), 1615 (s), 1454 (s), 1414 (s), 1327 (m), 1262 (m), 1186 (w), 1087 (w), 1017 (w), 960 (w), 897 (w), 748 (s), 716 (m), 597 (m), 478 (m), 424 cm⁻¹ (m); elemental analysis calcd (%) for C₉₀H₁₁₆N₁₇O₂₂NiTb: C 53.89, H 5.84, N 11.87, Tb 7.92; found: C 53.83, H 5.89, N 11.94, Tb 7.85.

Synthesis of IFMC-27-La, [Ni(L)La₂(NO₃)₃(dma)](NO₃)·2H₂O·2DMA: A mixture of H₄L (0.04 g, 0.36 mmol), NiCl₂·6H₂O (0.15 g, 0.63 mmol), La(NO₃)₃·6H₂O (0.04 g, 0.09 mmol), DMA (5 mL), and H₂O (2 mL) was sealed in a Teflon-lined stainless steel container and heated in an autoclave at 120°C for 4 days. The autoclave was cooled to room temperature, the container was removed, and 3 drops of HNO₃ were added. The container continued to be heated at 140°C for 4 days. After the autoclave was cooled to room temperature, light purple crystals were obtained, which were isolated by washing with DMA and dried at room temperature. Yield: 52% based on H₄L. IR (KBr): $\tilde{\nu}$ =3390 (s), 2934 (m), 1597 (s), 1548 (s), 1482 (s), 1452 (s), 1402 (s), 1329 (s), 1179 (w), 1111 (w), 1083 (w), 1016 (m), 941 (w), 894 (w), 854 (w), 765 (s), 743 (m), 714 (m), 667 (m), 611 (m), 474 cm⁻¹ (w); elemental analysis calcd (%) for C₇₈H₈₃N₁₇O₂₅NiLa₂: C 46.95, H 4.20, N 11.94, La 13.92; found: C 46.89, H 4.27, N 11.99, La 13.85.

Synthesis of the metalloligand [Ni_{0.5}(H₄L)_{0.5}](NO₃)·4CH₃CH₂OH: H₄L (0.02 g, 0.18 mmol) and Ni(NO₃)₂·6H₂O (0.08 g, 0.28 mmol) were each dissolved in ethanol (10 mL) with stirring. The two solutions were mixed in a 25 mL beaker and then three drops of HCl were added. The mixture was stirred for an additional 5 min and filtered to remove the precipitate. The clear solution was left in the air for 3 days. Light pink crystals were obtained, which were isolated by washing with ethanol and dried at room temperature. Yield: 59% based on H₄L. IR (KBr): $\tilde{\nu}$ =3381 (s), 1709 (s), 1614 (m), 1478 (s), 1453 (s), 1382 (s), 1178 (m), 1110 (m), 1041 (w), 1017 (w), 940 (w), 894 (w), 833 (m), 747 (s), 711 (m), 430 cm⁻¹ (w); elemental analysis calcd (%) for C₄₁H₅₂N₆O₁₁Ni_{0.5}: C 59.02, H 6.29, N 10.08; found: C 58.97, H 6.35, N 10.15.

Synthesis of IFMC-28-La, [Ni(L)La(H₂O)(dmf)₂](NO₃)·3H₂O·DMF: A mixture of the metalloligand (0.04 g, 0.05 mmol), La(NO₃)₃·6H₂O (0.07 g, 0.16 mmol), DMF (5 mL), and H₂O (3 mL) was sealed in a Teflon-lined stainless steel container. The container was heated to 110°C for 4 days resulting in light pink crystals, which were isolated by washing with DMF and dried at room temperature. Yield: 59% based on H₄L. IR (KBr): $\tilde{\nu}$ =3388 (s), 2924 (m), 1602 (s), 1546 (s), 1484 (s), 1452 (s), 1397 (s), 1328 (s), 1174 (m), 1110 (m), 1079 (m), 1013 (w), 927 (w), 892 (w), 856 (w), 747 (m), 527 (m), 421 cm⁻¹ (m); elemental analysis calcd (%) for C₇₂H₇₉N₁₂O₁₇NiLa: C 54.12, H 4.92, N 11.79, La 8.35; found: C 54.05, H 5.01, N 11.83, La 8.26.

Synthesis of IFMC-28-Eu, [Ni(L)Eu(H₂O)(dmf)₂](NO₃)·3H₂O·DMF: **IFMC-28-Eu** was synthesized by a procedure similar to that used for **IFMC-28-La** with Eu(NO₃)₃·6H₂O (0.05 g, 0.11 mmol) instead of La(NO₃)₃·6H₂O (0.07 g, 0.16 mmol). The light pink crystals were isolated by washing with DMF and dried at room temperature. Yield: 52% based on H₄L. IR (KBr): $\tilde{\nu}$ =3420 (s), 2933 (s), 1623 (s), 1556 (s), 1493 (s), 1403 (s), 1181 (m), 1108 (m), 1015 (m), 937 (w), 920 (w), 894 (w), 859 (s), 808 (w), 784 (m), 739 (s), 715 (m), 674 (w), 646 cm⁻¹ (w); elemental analysis calcd (%) for C₇₂H₇₉N₁₂O₁₇NiEu: C 54.70, H 4.88, N 11.69, Eu 9.06; found: C 54.63, H 4.95, N 11.78, Eu 9.01.

Synthesis of IFMC-28-Eu_{0.5}Tb_{0.4}, [Ni(L)Eu_{0.5}Tb_{0.4}(H₂O)(dmf)₂](NO₃)·3H₂O·DMF: **IFMC-28-Eu_{0.5}Tb_{0.4}** was synthesized by a procedure similar to that used for **IFMC-28-La** with Eu(NO₃)₃·6H₂O (0.05 g, 0.11 mmol) and Tb(NO₃)₃·6H₂O (0.03 g, 0.07 mmol) instead of La(NO₃)₃·6H₂O (0.07 g, 0.16 mmol). The light pink crystals were isolated by washing with DMA and dried at room temperature. Yield: 52% based on H₄L. IR (KBr): $\tilde{\nu}$ =3419 (s), 2933 (s), 1625 (s), 1478 (s), 1326 (s), 1180

(m), 1015 (m), 937 (w), 920 (w), 859 (m), 832 (w), 784 (m), 738 (s), 715 (m), 646 (w), 561 (w), 476 (w), 424 cm⁻¹ (m); elemental analysis calcd (%) for C₇₂H₇₉Ni₁₂O₁₇NiEu_{0.5}Tb_{0.4}: C 53.61, H 4.87, N 11.67, Eu 5.43, Tb 3.78; found: C 53.56, H 4.94, N 11.76, Eu 5.37, Tb 3.81.

Synthesis of IFMC-28-Eu_{0.5}Tb_{0.5}·[Ni(L)Eu_{0.5}Tb_{0.5}(H₂O)(dmf)₂]·(NO₃)₃·3H₂O·DMF: IFMC-28-Eu_{0.5}Tb_{0.5} was synthesized by a procedure similar to that used for IFMC-28-La with Eu(NO₃)₃·6H₂O (0.04 g, 0.09 mmol) and Tb(NO₃)₃·6H₂O (0.04 g, 0.11 mmol) instead of La(NO₃)₃·6H₂O (0.07 g, 0.16 mmol). The light pink crystals were isolated by washing with DMA and dried at room temperature. Yield: 53% based on H₄L. IR (KBr): $\bar{\nu}$ =3419 (s), 2932 (s), 1625 (s), 1543 (s), 1478 (s), 1327 (s), 1181 (m), 1015 (m), 920 (w), 807 (w), 784 (m), 739 (s), 715 (m), 675 (w), 646 (w), 593 (w), 477 (w), 424 cm⁻¹ (m); elemental analysis calcd (%) for C₇₂H₇₉Ni₁₂O₁₇NiEu_{0.5}Tb_{0.5}: C 53.59, H 4.87, N 11.67, Eu 4.52, Tb 4.73; found: C 53.53, H 4.92, N 11.73, Eu 4.46, Tb 4.66.

Synthesis of IFMC-28-Eu_{0.4}Tb_{0.6}·[Ni(L)Eu_{0.4}Tb_{0.6}(H₂O)(dmf)₂]·(NO₃)₃·3H₂O·DMF: IFMC-28-Eu_{0.4}Tb_{0.6} was synthesized by a procedure similar to that used for IFMC-28-La with Eu(NO₃)₃·6H₂O (0.03 g, 0.07 mmol) and Tb(NO₃)₃·6H₂O (0.05 g, 0.11 mmol) instead of La(NO₃)₃·6H₂O (0.07 g, 0.16 mmol). The light pink crystals were isolated by washing with DMA and dried at room temperature. Yield: 54% based on H₄L. IR (KBr): $\bar{\nu}$ =3408 (s), 2932 (s), 1616 (s), 1478 (s), 1414 (s), 1180 (m), 1162 (m), 1108 (m), 949 (w), 920 (w), 894 (m), 831 (w), 808 (w), 784 (m), 751 (s), 715 (m), 646 (w), 611 (w), 424 cm⁻¹ (m); elemental analysis calcd (%) for C₇₂H₇₉Ni₁₂O₁₇NiEu_{0.4}Tb_{0.6}: C 53.57, H 4.87, N 11.66, Eu 3.61, Tb 5.67; found: C 53.49, H 4.94, N 11.74, Eu 3.56, Tb 5.49.

Synthesis of IFMC-28-Tb, [Ni(L)Tb(H₂O)(dmf)₂]·(NO₃)₃·3H₂O·DMF: IFMC-28-Tb was synthesized by a procedure similar to that used for IFMC-28-La with Tb(NO₃)₃·6H₂O (0.05 g, 0.11 mmol) instead of La(NO₃)₃·6H₂O (0.07 g, 0.16 mmol). The light pink crystals were isolated by washing with DMA and dried at room temperature. Yield: 53% based on H₄L. IR (KBr): $\bar{\nu}$ =3448 (s), 2934 (s), 1633 (s), 1497 (s), 1265 (s), 1188 (m), 1107 (w), 1081 (m), 1016 (s), 939 (w), 860 (w), 831 (w), 746 (m), 715 (m), 645 (w), 592 (m), 475 (m), 424 cm⁻¹ (m); elemental analysis calcd (%) for C₇₂H₇₉Ni₁₂O₁₇NiTb: C 53.48, H 4.86, N 11.65, Tb 9.44; found: C 53.43, H 4.93, N 11.72, Tb 9.38.

X-ray crystallography: Single-crystal X-ray diffraction data were recorded on a Bruker APEXII CCD diffractometer with graphite-monochromated Mo_{Kα} radiation ($\lambda=0.71069\text{ \AA}$) at 293 K. Absorption corrections were applied by using the multiscan technique. All the structures were solved by the Direct Method of SHELXS-97 and refined by full-matrix least-squares techniques using the SHELXL-97 program within WINGX. The solvent molecules are highly disordered, and attempts to locate and refine the solvent peaks were unsuccessful. Contributions to scattering due to these solvent molecules were removed by using the SQUEEZE routine of PLATON; structures were then refined again using the data generated. Crystal data are summarized in Table S1 in the Supporting Information. CCDC-921351 (IFMC-26-Eu), 921352 (IFMC-27-La), 921353 (IFMC-28-La), 921354 (the metalloligand), and 921355 (IFMC-26-Tb) contain the supplementary crystallographic data for this paper. These data can be obtained free of charge from The Cambridge Crystallographic Data Centre via www.ccdc.cam.ac.uk/data_request/cif.

Acknowledgements

This work was financially supported by Pre-973 Program (2010CB635114), the National Natural Science Foundation of China (Nos. 21001020 and 21271089), and the program of Jiangsu Specially Appointed Professor, the project funded by the Priority Academic Program Development of Jiangsu Higher Education Institutions, and Graduate Innovation Fund of Jilin University (No. 20121048).

[1] a) M. Eddaoudi, J. Kim, N. Rosi, D. Vodak, J. Wachter, M. O’Keeffe, O. M. Yaghi, *Science* **2002**, *295*, 469–472; b) S. C. Xiang, Z. J. Zhang, C. G. Zhao, K. L. Hong, X. B. Zhao, D. R. Ding, M. H.

Xie, C. D. Wu, M. C. Das, R. Gill, K. M. Thomas, B. L. Chen, *Nat. Commun.* **2011**, *2*, 204–210; c) Z. Y. Guo, H. Wu, G. Srinivas, Y. M. Zhou, S. C. Xiang, Z. X. Chen, Y. T. Yang, W. Zhou, M. O’Keeffe, B. L. Chen, *Angew. Chem.* **2011**, *123*, 3236–3239; *Angew. Chem. Int. Ed.* **2011**, *50*, 3178–3181; d) Y. E. Cheon, M. P. Suh, *Angew. Chem.* **2009**, *121*, 2943–2947; *Angew. Chem. Int. Ed.* **2009**, *48*, 2899–2903; e) H. L. Jiang, T. Akita, T. Ishida, M. Haruta, Q. Xu, *J. Am. Chem. Soc.* **2011**, *133*, 1304–1306; f) F. Wang, Y. X. Tan, H. Yang, H. X. Zhang, Y. Kang, J. Zhang, *Chem. Commun.* **2011**, *47*, 5828–5830; g) J. S. Qin, D. Y. Du, W. L. Li, J. P. Zhang, S. L. Li, Z. M. Su, X. L. Wang, Q. Xu, K. Z. Shao, Y. Q. Lan, *Chem. Sci.* **2012**, *3*, 2114–2118; h) J. A. Mason, K. Sumida, Z. R. Herm, R. Krishna, J. R. Long, *Energy Environ. Sci.* **2011**, *4*, 3030–3040; i) S. Liu, Z. Xiang, Z. Hu, X. Zheng, D. Cao, *J. Mater. Chem.* **2011**, *21*, 6649–6653; j) W. G. Lu, D. Q. Yuan, T. A. Makal, J. R. Li, H. C. Zhou, *Angew. Chem.* **2012**, *124*, 1612–1616; *Angew. Chem. Int. Ed.* **2012**, *51*, 1580–1584; k) Y. N. Gong, M. Meng, D. C. Zhong, Y. L. Huang, L. Jiang, T. B. Lu, *Chem. Commun.* **2012**, *48*, 12002–12004; l) P. Pachfule, Y. F. Chen, J. W. Jiang, R. Banerjee, *Chem. Eur. J.* **2012**, *18*, 688–694.

- [2] a) J. R. Li, H. C. Zhou, *Nat. Chem.* **2010**, *2*, 893–898; b) C. Y. Sun, C. Qin, C. G. Wang, Z. M. Su, S. Wang, X. L. Wang, G. S. Yang, K. Z. Shao, Y. Q. Lan, E. B. Wang, *Adv. Mater.* **2011**, *23*, 5629–5632; c) D. Zhao, S. W. Tan, D. Q. Yuan, W. G. Lu, Y. H. Rezenom, H. L. Jiang, L. Q. Wang, H. C. Zhou, *Adv. Mater.* **2011**, *23*, 90–93; d) Z. Ma, B. Moulton, *Coord. Chem. Rev.* **2011**, *255*, 1623–1641; e) F. Ke, Y. P. Yuan, L. G. Qiu, Y. H. Shen, A. J. Xie, J. F. Zhu, X. Y. Tian, L. D. Zhang, *J. Mater. Chem.* **2011**, *21*, 3843–3848; f) R. C. Huxford, J. D. Rocca, W. Lin, *Curr. Opin. Chem. Biol.* **2010**, *14*, 262–268; g) D. Y. Du, J. S. Qin, T. T. Wang, S. L. Li, Z. M. Su, K. Z. Shao, Y. Q. Lan, X. L. Wang, E. B. Wang, *Chem. Sci.* **2012**, *3*, 705–710; h) X. Zhu, H. Y. Zheng, X. F. Wei, Z. Y. Lin, L. G. Guo, B. Qiu, G. N. Chen, *Chem. Commun.* **2013**, *49*, 1276–1278; i) D. Hermann, H. Emerich, R. Lepski, D. Schaniel, U. Ruschewitz, *Inorg. Chem.* **2013**, *52*, 2744–2749.
- [3] a) P. Falcaro, S. Furukawa, *Angew. Chem.* **2012**, *124*, 8557–8559; *Angew. Chem. Int. Ed.* **2012**, *51*, 8431–8433; b) A. Zaïm, H. Nozary, L. Guénée, C. Besnard, J. Lemonnier, S. Petoud, C. Piguet, *Chem. Eur. J.* **2012**, *18*, 7155–7168; c) H. H. Li, W. Shi, K. N. Zhao, Z. Niu, H. M. Li, P. Cheng, *Chem. Eur. J.* **2013**, *19*, 3358–3365; d) P. R. Matthes, C. J. Höller, M. Mai, J. Heck, S. J. Sedlmaier, S. Schmiechen, C. Feldmann, W. Schnick, K. Müller-Buschbaum, *J. Mater. Chem.* **2012**, *22*, 10179–10187; e) C. J. Höller, K. Müller-Buschbaum, *Inorg. Chem.* **2008**, *47*, 10141–10149; f) R. Decadt, K. V. Hecke, D. Depla, K. Leus, D. Weinberger, I. V. Driesche, P. V. D. Voort, R. V. Deun, *Inorg. Chem.* **2012**, *51*, 11623–11634; g) H. B. Zhang, X. C. Shan, L. J. Zhou, P. Lin, R. F. Li, E. Ma, X. G. Guo, S. W. Du, *J. Mater. Chem. C* **2013**, *1*, 888–891.
- [4] a) B. L. Chen, L. B. Wang, Y. Q. Xiao, F. R. Fronczek, M. Xue, Y. J. Cui, G. D. Qian, *Angew. Chem.* **2009**, *121*, 508–511; *Angew. Chem. Int. Ed.* **2009**, *48*, 500–503; b) B. L. Chen, L. B. Wang, F. Zapata, G. D. Qian, E. B. Lobkovsky, *J. Am. Chem. Soc.* **2008**, *130*, 6718–6719; c) M. P. Suh, Y. Cheon, E. Lee, *Coord. Chem. Rev.* **2008**, *252*, 1007–1026; d) J. Rocha, L. D. Carlos, F. A. A. Paz, D. Ananias, *Chem. Soc. Rev.* **2011**, *40*, 926–940; e) B. Chen, S. Xiang, G. Qian, *Acc. Chem. Res.* **2010**, *43*, 1115–1124; f) O. Shekhah, J. Liu, R. A. Fischer, C. Wöll, *Chem. Soc. Rev.* **2011**, *40*, 1081–1106; g) G. Férey, *Chem. Soc. Rev.* **2008**, *37*, 191–214; h) R. J. Kuppler, D. J. Timmons, Q. R. Fang, J. R. Li, T. A. Makal, M. D. Young, D. Yuan, D. Zhao, W. Zhuang, H. C. Zhou, *Coord. Chem. Rev.* **2009**, *253*, 3042–3066; i) L. Chen, K. Tan, Y. Q. Lan, S. L. Li, K. Z. Shao, Z. M. Su, *Chem. Commun.* **2012**, *48*, 5919–5921; j) F. Y. Yi, W. T. Yang, Z. M. Sun, *J. Mater. Chem.* **2012**, *22*, 23201–23209; k) S. Dang, E. Ma, Z. M. Sun, H. J. Zhang, *J. Mater. Chem.* **2012**, *22*, 16920–16926.
- [5] Y. J. Cui, Y. F. Yue, G. D. Qian, B. L. Chen, *Chem. Rev.* **2012**, *112*, 1126–1162.
- [6] a) D. Buso, J. Jasieniak, M. D. H. Lay, P. Schiavuta, P. Scopece, J. Laird, H. Amenitsch, A. J. Hill, P. Falcaro, *Small* **2012**, *8*, 80–88; b) S. Jin, H. J. Son, O. K. Farha, G. P. Wiederrecht, J. T. Hupp, *J. Am. Chem. Soc.* **2013**, *135*, 955–958.

- [7] a) S. Dang, J. H. Zhang, Z. M. Sun, *J. Mater. Chem.* **2012**, *22*, 8868–8873; b) G. J. He, D. Guo, C. He, X. L. Zhang, X. W. Zhao, C. Y. Duan, *Angew. Chem.* **2009**, *121*, 6248–6251; *Angew. Chem. Int. Ed.* **2009**, *48*, 6132–6135; c) L. Li, S. Q. Zhang, L. Han, Z. H. Sun, J. H. Luo, M. C. Hong, *Cryst. Growth Des.* **2013**, *13*, 106–110; d) B. A. Blight, R. Guillet-Nicolas, F. Kleitz, R. Y. Wang, S. N. Wang, *Inorg. Chem.* **2013**, *52*, 1673–1675.
- [8] a) B. V. Harbuzaru, A. Corma, F. Rey, J. L. Jordá, D. Ananias, L. D. Carlos, J. Rocha, *Angew. Chem.* **2009**, *121*, 6598–6601; *Angew. Chem. Int. Ed.* **2009**, *48*, 6476–6479; b) Y. J. Cui, H. Xu, Y. F. Yue, Z. Y. Guo, J. C. Yu, Z. X. Chen, J. K. Gao, Y. Yang, G. D. Qian, B. L. Chen, *J. Am. Chem. Soc.* **2012**, *134*, 3979–3982; c) R. M. P. Colodrero, K. E. Papathanasiou, N. Stavgianoudaki, P. Olivera-Pastor, E. R. Losilla, M. A. G. Aranda, L. León-Reina, J. Sanz, I. Sobrados, D. Choquesillo-Lazarte, J. M. García-Ruiz, P. Atienzar, F. Rey, K. D. Demadis, A. Cabeza, *Chem. Mater.* **2012**, *24*, 3780–3792.
- [9] a) J. An, C. M. Shade, D. A. Chengelis-Czegan, S. Petoud, N. L. Rosi, *J. Am. Chem. Soc.* **2011**, *133*, 1220–1223; b) Y. Q. Lan, H. L. Jiang, S. L. Li, Q. Xu, *Adv. Mater.* **2011**, *23*, 5015–5020; c) W. W. He, S. L. Li, G. S. Yang, Y. Q. Lan, Z. M. Su, Q. Fu, *Chem. Commun.* **2012**, *48*, 10001–10003; d) D. F. Sava, L. E. S. Rohwer, M. A. Rodriguez, T. M. Nenoff, *J. Am. Chem. Soc.* **2012**, *134*, 3983–3986.
- [10] a) M. D. Allendorf, C. A. Bauer, R. K. Bhakta, R. J. Houk, *Chem. Soc. Rev.* **2009**, *38*, 1330–1352; b) D. P. Yan, G. O. Lloyd, A. Delori, W. Jones, X. Duan, *ChemPlusChem* **2012**, *77*, 1112–1118; c) C. Serre, F. Millange, C. Thouvenot, N. Gardant, F. Pellé, G. Férey, *J. Mater. Chem.* **2004**, *14*, 1540–1543; d) W. J. Rieter, K. M. L. Taylor, H. An, W. Lin, W. Lin, *J. Am. Chem. Soc.* **2006**, *128*, 9024–9025; e) K. C. Stylianou, R. Heck, S. Y. Chong, J. Bacsá, J. T. A. Jones, Y. Z. Khimyak, D. Bradshaw, M. J. Rosseinsky, *J. Am. Chem. Soc.* **2010**, *132*, 4119–4130.
- [11] T. Gadzikwa, G. Lu, C. L. Stern, S. R. Wilson, J. T. Hupp, S. T. Nguyen, *Chem. Commun.* **2008**, 5493–5495.
- [12] A. C. Sudik, A. P. Côté, A. G. Wong-Foy, M. O’Keeffe, O. M. Yaghi, *Angew. Chem.* **2006**, *118*, 2590–2595; *Angew. Chem. Int. Ed.* **2006**, *45*, 2528–2533.
- [13] a) P. Thanasekaran, C. C. Lee, K. L. Lu, *Acc. Chem. Res.* **2012**, *45*, 1403–1418; b) B. J. Burnett, P. M. Barron, C. Hu, W. Choe, *J. Am. Chem. Soc.* **2011**, *133*, 9984–9987; c) Z. Zhang, S. Xiang, Y. S. Chen, S. Ma, Y. Lee, T. Phely-Bobin, B. Chen, *Inorg. Chem.* **2010**, *49*, 8444–8448.
- [14] a) Y. Q. Lan, S. L. Li, H. L. Jiang, Q. Xu, *Chem. Eur. J.* **2012**, *18*, 8076–8083; b) X. L. Wang, C. Qin, S. X. Wu, K. Z. Shao, Y. Q. Lan, S. Wang, D. X. Zhu, Z. M. Su, E. B. Wang, *Angew. Chem.* **2009**, *121*, 5395–5399; *Angew. Chem. Int. Ed.* **2009**, *48*, 5291–5295; c) J. R. Li, D. J. Timmons, H. C. Zhou, *J. Am. Chem. Soc.* **2009**, *131*, 6368–6369; d) A. Schoedel, L. Wojtas, S. P. Kelley, R. D. Rogers, M. Eddaoui, M. J. Zaworotko, *Angew. Chem.* **2011**, *123*, 11623–11626; *Angew. Chem. Int. Ed.* **2011**, *50*, 11421–11424; e) H. N. Wang, X. Meng, G. S. Yang, X. L. Wang, K. Z. Shao, Z. M. Su, C. G. Wang, *Chem. Commun.* **2011**, *47*, 7128–7130.
- [15] Y. L. Bai, J. Tao, R. B. Huang, L. S. Zheng, *Angew. Chem.* **2008**, *120*, 5424–5427; *Angew. Chem. Int. Ed.* **2008**, *47*, 5344–5347.
- [16] M. C. Das, Q. S. Guo, Y. B. He, J. Kim, C. G. Zhao, K. L. Hong, S. C. Xiang, Z. J. Zhang, K. M. Thomas, R. Krishna, B. L. Chen, *J. Am. Chem. Soc.* **2012**, *134*, 8703–8710.
- [17] M. C. Das, S. C. Xiang, Z. J. Zhang, B. L. Chen, *Angew. Chem.* **2011**, *123*, 10696–10707; *Angew. Chem. Int. Ed.* **2011**, *50*, 10510–10520.
- [18] a) S. R. Halper, L. Do, J. R. Stork, S. M. Cohen, *J. Am. Chem. Soc.* **2006**, *128*, 15255–15268; b) D. W. Smithery, S. R. Wilson, K. S. Suslick, *Inorg. Chem.* **2003**, *42*, 7719–7721; c) K. S. Suslick, P. Bhyrappa, J. H. Chou, M. E. Kosal, S. Nakagaki, D. W. Smithery, S. R. Wilson, *Acc. Chem. Res.* **2005**, *38*, 283–291; d) R. Kitaura, G. Onoyama, H. Sakamoto, R. Matsuda, S. Noro, S. Kitagawa, *Angew. Chem.* **2004**, *116*, 2738–2741; *Angew. Chem. Int. Ed.* **2004**, *43*, 2684–2687.
- [19] a) H. S. Liu, Y. Q. Lan, S. L. Li, *Cryst. Growth Des.* **2010**, *10*, 5221–5226; b) D. Y. Du, J. S. Qin, C. X. Sun, X. L. Wang, S. R. Zhang, P. Shen, S. L. Li, Z. M. Su, Y. Q. Lan, *J. Mater. Chem.* **2012**, *22*, 19673–19678.
- [20] a) P. Benndorf, S. Schmitt, R. Köppe, P. Oña-Burgos, A. Scheurer, K. Meyer, P. W. Roesky, *Angew. Chem.* **2012**, *124*, 5091–5095; *Angew. Chem. Int. Ed.* **2012**, *51*, 5006–5010; b) H. L. Jiang, N. Tsunomori, Q. Xu, *Inorg. Chem.* **2010**, *49*, 10001–10006; c) H. Wang, S. J. Liu, D. Tian, J. M. Jia, T. L. Hu, *Cryst. Growth Des.* **2012**, *12*, 3263–3270; d) D. Y. Du, J. S. Qin, S. L. Li, Y. Q. Lan, X. L. Wang, Z. M. Su, *Aust. J. Chem.* **2010**, *63*, 1389–1395.
- [21] a) S. Dang, J. H. Zhang, Z. M. Sun, H. J. Zhang, *Chem. Commun.* **2012**, *48*, 11139–11141; b) X. Ma, X. Li, Y. E. Cha, L. P. Jin, *Cryst. Growth Des.* **2012**, *12*, 5227–5232.
- [22] a) Y. Q. Sun, J. Zhang, Y. M. Chen, G. Y. Yang, *Angew. Chem.* **2005**, *117*, 5964–5967; *Angew. Chem. Int. Ed.* **2005**, *44*, 5814–5817; b) J. W. Cheng, S. T. Zheng, G. Y. Yang, *Dalton Trans.* **2007**, 4059–4066.
- [23] T. Gunnlaugsson, J. P. Leonard, *Chem. Commun.* **2005**, 3114–3131.
- [24] a) F. S. Richardson, *Chem. Rev.* **1982**, *82*, 541–552; b) J. S. Qin, D. Y. Du, L. Chen, X. Y. Sun, Y. Q. Lan, Z. M. Su, *J. Solid State Chem.* **2011**, *184*, 373–378.

Received: April 22, 2013

Published online: July 12, 2013